

Dust evolution during protoplanetary disk buildup enhances CO ice relative to water

J. Drażkowska* 

Max Planck Institute for Solar System Research, Justus-von-Liebig-Weg 3, 37077 Göttingen, Germany

Received 27 January 2026 / Accepted 25 March 2026

ABSTRACT

Context. Water ice is expected to be the dominant volatile component of bodies formed in the outer Solar System. However, recent observations of comets and trans-Neptunian objects suggest that the relative abundances of ices can vary substantially, with some bodies exhibiting unusually high CO/H₂O ratios.

Aims. We studied the prospects of CO-rich pebbles and planetesimals being produced.

Methods. We used a one-dimensional protoplanetary disk model with dust evolution including coagulation, fragmentation, and radial drift; water and CO ice and vapor evolution; and planetesimal formation via the streaming instability. We compared models with and without the disk formation stage.

Results. CO-rich pebbles can form at the CO snow line due to the cold-finger effect, regardless of whether the disk buildup is included. Models including disk buildup show stronger CO enhancement relative to water in the outer disk. However, CO-rich planetesimals do not form in the smooth disk models.

Conclusions. The formation of CO-rich planetesimals likely requires mechanisms that preserve the CO-enriched ice reservoir, such as pressure traps or gas removal processes. Models dealing with the chemical evolution of protoplanetary disks and its impact on the atmospheric C/O ratio of forming planets should consider the disk buildup stage.

Key words. planets and satellites: formation – protoplanetary disks

1. Introduction

Water is nominally considered the most abundant volatile in the Solar System. Comets forming in the cold outer region of the solar nebula are expected to be a mix of refractory and icy dust species; water ice dominates the mixture with an abundance of over 50% (Lodders 2003). However, some of the known comets seem to be dominated by CO ice rather than water ice. C/2009 P1 (Garradd) was the first comet for which a significant CO/H₂O production rate was observed inside the water snow line (Feaga et al. 2014). Although it did not cross inside the water snow line, C/2006 W3 (Christensen) is also suspected to have a high CO abundance based on its production rate (Boney et al. 2017). C/2016 R2 (PanSTARRS) is the canonical example of a comet with CO dominating the volatile budget with an estimated CO/H₂O ratio as high as 300 (Biver et al. 2018; McKay et al. 2019; Harrington Pinto et al. 2022). The interstellar comet 2I/Borisov showed unusually high CO compared to typical Solar System comets (Cordiner et al. 2020; Bodewits et al. 2020). The recent JWST observations revealed distinct surface compositions of the trans-Neptunian objects; water ice was not universally present, suggesting their compositional diversity (Pinilla-Alonso et al. 2025; De Prá et al. 2025).

The meteoritic evidence also suggests that water was not always the dominant ice component in the carbonaceous chondrite parent bodies that formed beyond the water ice line. The initial water-to-rock ratio varied from 0.01 to above 1 in different carbonaceous chondrite classes (Brearley 2006; Marrocchi et al. 2018). Sridhar et al. (2021) showed that some of the

carbonaceous chondrite parent bodies, in particular Renazzo-type (CR) and the ungrouped Tagish Lake (TL) chondrites, must have included a significant fraction of ammonia ice as they were altered by the action of an ammonia-bearing fluid based on the distinct magnetite morphologies corresponding to different aqueous alteration pathways found in those meteorites.

Clathration is often discussed as a possible process that locally concentrates CO and other volatiles in comets. In the protoplanetary disk, CO can become trapped in the water ice more efficiently than expected from equilibrium condensation alone (Bar-Nun et al. 1985; Mousis et al. 2010). When a cometary nucleus made of such clathrates warms up, the trapped CO is released preferentially, increasing the observed CO/H₂O ratio. However, Mousis et al. (2021) showed that the amount of water required by clathration to match the N₂/CO ratio measured for C/2016 R2 (PanSTARRS) is inconsistent with its estimated low abundance.

Price et al. (2021) and Mousis et al. (2021) proposed that an increase in CO is expected locally in the vicinity of the CO evaporation front due to the cold-finger effect: the recondensation of CO vapor diffusing outward across the CO condensation line. However, these models start the ice and vapor evolution from a fully fledged disk, neglecting the disk buildup stage. In this paper, we revisit the expected CO enhancement using a model including the protoplanetary disk formation stage and compare the results to a model starting with a fully fledged disk.

This paper is organized as follows. We present the numerical setup in Sect. 2. We present the results of our models in Sect. 3. We discuss the limitations of the numerical approach and implications of the results in Sect. 4. Section 5 concludes this work.

* Corresponding author: drazkowska@mps.mpg.de

2. Methods

We built a one-dimensional model of a protoplanetary disk following the methodology presented in Drążkowska & Dullemond (2018) (hereafter DD18). The protoplanetary disk formation was considered by the infall of the spherically symmetric rotating molecular cloud (Shu 1977; Ulrich 1976; Hueso & Guillot 2005). We considered a molecular cloud of one solar mass rotating at the rate of $\Omega = 7 \cdot 10^{-15} \text{ s}^{-1}$, which ends up forming a single star and the surrounding protoplanetary disk, which reaches its peak mass of $0.25 M_{\odot}$ after 0.64 Myr since the beginning of the infall simulation, which we call time zero when analyzing the results. The infall proceeds inside-out such that initially the material accretes directly onto the star and the centrifugal radius crosses the inner boundary of the disk about 0.14 Myr after the start of the model, corresponding to time -0.5 Myr marked in the figures. We assume that the disk has an intrinsic turbulence prescribed with $\alpha = 10^{-3}$ and that its temperature structure is set both by the viscous heating and irradiation from the central star.

We ran sets of two models, one initializing dust at a constant dust-to-gas ratio across the disk when the gas disk is at its maximum mass (models without disk buildup) and a corresponding model where dust evolution was considered from the very beginning, when the first material arrived at the disk (models with disk buildup). The dust has three components: refractory dust with 0.5% mass ratio, water ice with 0.5% mass ratio, and CO ice with 0.14% mass ratio with respect to the gas. We assume that dust aggregates are spherical and that there is one typical grain size a_p at each radial distance, which is calculated according to the same procedure as in DD18, including initial growth phase, fragmentation, and radial drift, similar to the two-population model proposed by Birnstiel et al. (2012). We assume that the fragmentation speed is 10 m s^{-1} outside and 1 m s^{-1} inside of the water snow line with a smooth transition in between. The dust surface density of each dust component is evolved by radial drift, advection with the gas flow, and diffusion. As in DD18, the water ice can evaporate to water vapor, which can recondense back to water ice.

We extended the model presented by DD18 to include the CO ice and vapor evolution. In the same way as for water, we calculated the equilibrium pressure of CO at every location of the disk

$$P_{\text{eq}}^{\text{CO}} = P_{\text{eq},0}^{\text{CO}} e^{-T_a^{\text{CO}}/T}, \quad (1)$$

where we adopted $P_{\text{eq},0}^{\text{CO}} = 7.73 \cdot 10^{11} \text{ g cm}^{-1} \text{ s}^{-2}$ and $T_a^{\text{CO}} = 1030 \text{ K}$ following Leger et al. (1985), consistent with later laboratory determinations.

We followed the evolution of the surface density of CO ice $\Sigma_{\text{ice}}^{\text{CO}}$, which changes together with the other dust species by the radial drift, advection with gas flow, and diffusion, and the evolution of the CO vapor $\Sigma_{\text{vap}}^{\text{CO}}$, which evolves according to the accretion flow of gas and diffusion. Adopting the approach that Schoonenberg & Ormel (2017) proposed for water, $\Sigma_{\text{ice}}^{\text{CO}}$ and $\Sigma_{\text{vap}}^{\text{CO}}$ also change due to CO condensation and evaporation, and the rate of this change is given by

$$\dot{\Sigma}_{\text{ice}}^{\text{CO}} = -\dot{\Sigma}_{\text{vap}}^{\text{CO}} = R_c \Sigma_{\text{ice}}^{\text{CO}} \Sigma_{\text{vap}}^{\text{CO}} - R_e \Sigma_{\text{ice}}^{\text{CO}}, \quad (2)$$

where the condensation and evaporation rates are defined as

$$R_c = 6 \sqrt{\frac{k_B T}{\mu_{\text{CO}} \pi a_p \rho_p H_g}} \quad (3)$$

and

$$R_e = 6 \sqrt{\frac{2\pi\mu_{\text{CO}}}{k_B T}} \frac{P_{\text{eq}}^{\text{CO}}}{\pi a_p \rho_p}, \quad (4)$$

where k_B is the Boltzmann constant; T is the midplane disk temperature; $\mu_{\text{CO}} = 28m_H$, with m_H the proton mass and μ_{CO} the weight of the CO molecule; a_p and ρ_p are dust grain radius and material density, and H_g is disk scale-height. It is worth noting that both the condensation and evaporation rates increase when the dust grains are smaller.

We used 1000 logarithmically spaced radial cells to cover the radial grid stretching from 0.3 au to 10 pc. We ran the model until 3 Myr after the time the disk reached its peak mass (start of the model without disk buildup)¹.

3. Results

3.1. Fiducial model

Figure 1 shows the evolution of the total dust surface density, i.e., the sum of refractory dust and ice components, in the run without and with dust evolution during buildup taken into account. The two models evolve in a similar way; the main difference is a slightly faster inner disk depletion in the model including disk buildup. This is caused by the dust evolution during the buildup phase lasting over 0.5 Myr. Because the dust already had time to grow and drift inward, there is more dust in the inner disk, and the outer disk is already depleted compared to the run in which the dust is only initialized at the time of maximum gas disk mass (marked as time zero in the plots). This leads to the inner disk being depleted in dust faster than in the run without disk buildup, consistent with the conclusion reached in Birnstiel et al. (2010).

We define the location of the water and CO snow lines as the radial distance where 50% of the total surface density of the respective species is in the gas phase and 50% in the solid phase. The position of the water and CO snow lines is practically identical in the two models as they share the same temperature structure, which is independent of dust surface density and maximum grain size. The water snow line is located in the part of the disk where temperature is set by viscous heating, and it moves inward with time as the disk becomes less massive and cools down. On the contrary, the position of the CO snow line does not change significantly during the disk evolution, as it is located in the irradiation-dominated part of the disk, and we do not include stellar luminosity evolution. This is consistent with findings of the earlier work of Stammler et al. (2017). The local increase in the solid surface density that is visible outside of both the snow lines is caused by the cold-finger effect, with additional contribution of the traffic jam effect in the case of the H₂O snow line (see Drążkowska & Alibert (2017) and DD18 for details). In agreement with the results of DD18, we find no planetesimal formation in the models assuming the global isotropic turbulence with $\alpha = 10^{-3}$.

It is worth noting that in the model with disk buildup, the centrifugal radius shifts from inside to outside of the water snow line during the infall phase. As a result, water delivered early in the buildup is deposited inside the snow line in vapor form and later recondenses, whereas material accreted after the centrifugal radius has moved outward arrives as primordial ice. Presence of primordial water ice seems to be necessary to explain the

¹ The numerical code used to produce results presented in this paper is available at <https://github.com/astrojoanna/DD-diskevol-CO>

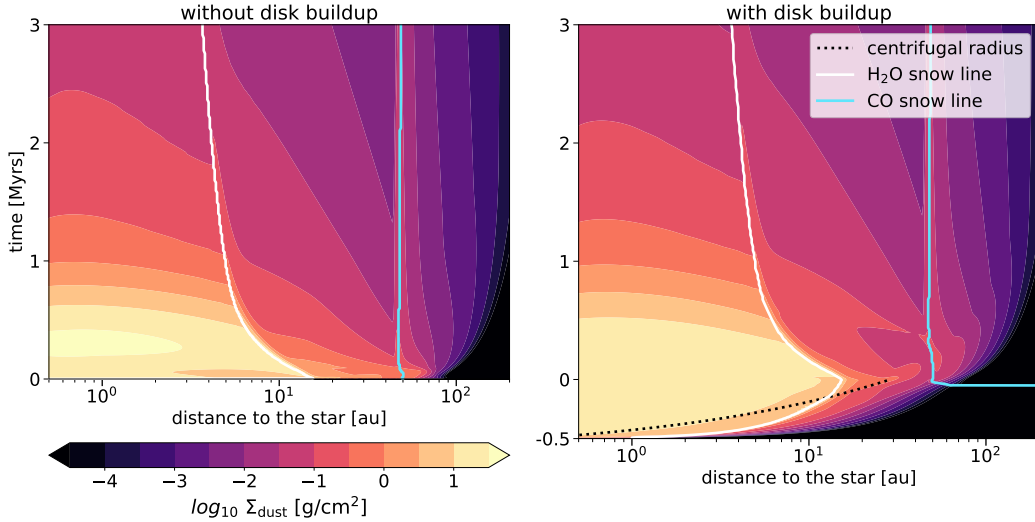


Fig. 1. Dust surface density evolution in the fiducial model without disk buildup (left) and with disk buildup taken into account (right). Time zero refers to the moment the gas disk reaches maximum mass in the model including its buildup, corresponding to the time the dust is initialized in the model without disk buildup.

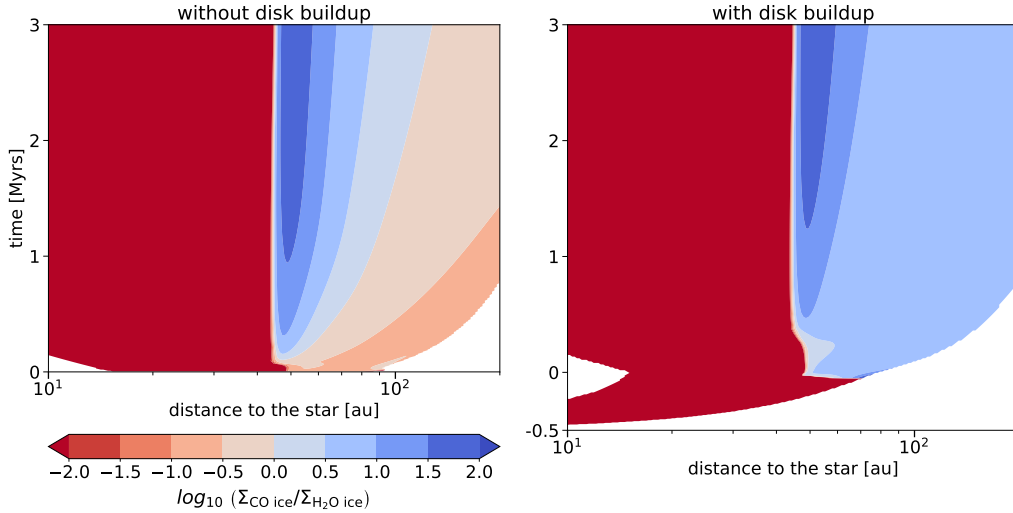


Fig. 2. Evolution of the CO-to-H₂O ice ratio as a function of time and space in the fiducial model without disk buildup (left) and with disk buildup taken into account (right). We note that the x-axis is different from that in Fig. 1 as this figure is centered at the CO snow line.

deuterium-to-hydrogen enrichment of water in the Solar System (Cleeves et al. 2014). However, the situation is different for CO, as the CO snow line remains outside of the centrifugal radius at all times, and thus the primordial CO ice evaporates during the infall phase and recondenses when the CO vapor is carried outside of the CO snow line, in agreement with the findings of the 2D model presented by Visser et al. (2009). Thus, the abundance of CO ice is solely regulated by its condensation rate, whereas the water ice reservoir reflects both primordial delivery and recondensation. This difference in origin and regulation underlies the distinct behavior of CO and water ice abundances presented below.

Figure 2 shows the evolution of the ratio of CO ice to water ice surface density in both models. Here we observe a significant difference between the two runs. In the model without disk buildup, there is a cold-finger-driven enhancement of CO ice outside of the CO snow line exceeding a factor of 10 after 1 Myr of evolution, but the CO/H₂O ratio gradually decreases with radial distance to the fiducial value of 0.28 (corresponding

to the log₁₀ value of -0.55 in the figures), consistent with the earlier results of Price et al. (2021) and Mousis et al. (2021). However, in the model including disk buildup, the whole region outside of the CO snow line becomes dominated by the CO ice, with the CO/H₂O ratio of 3. The reason for this difference is illustrated in Fig. 3. Due to dust evolution during disk buildup, the outer disk is depleted in solids compared to the model in which dust evolution starts when the disk is fully formed. This is reflected in the lower water ice density (left panel of Fig. 3), and the consequence is the smaller dust grain size (right panel of Fig. 3). The dust size is smaller because the lower dust-to-gas ratio leads to slower dust growth and a stronger radial drift barrier (see, e.g., Birnstiel et al. 2012). However, since the condensation rate given by Eq. (3) is higher for the smaller grain size, a larger fraction of the CO reservoir is transferred from the gas to the solid phase via freeze-out compared to the model without buildup, leading to a higher surface density of CO ice (see the middle panel of Fig. 3). This is promoted by the fact that the centrifugal radius is inside the CO snow line, and thus the CO

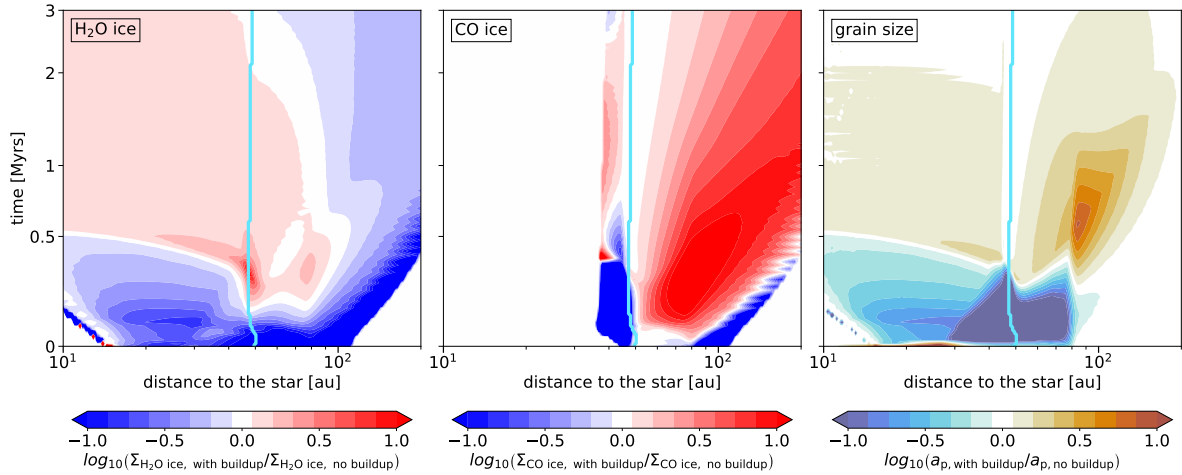


Fig. 3. Difference between the evolution of the surface density of H₂O ice (left), CO ice (middle), and dust grain size (right) between the runs with and without disk buildup. The vertical blue line marks the location of the CO snow line.

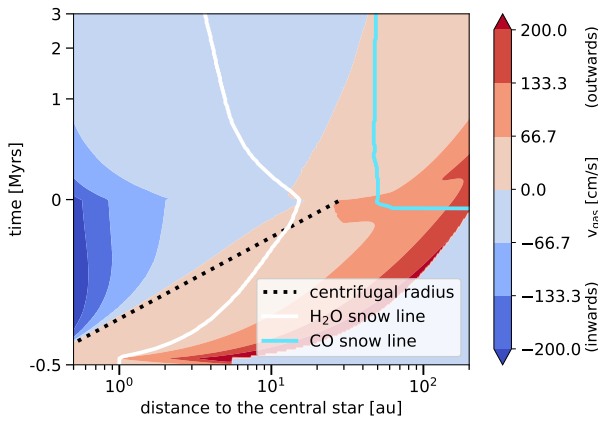


Fig. 4. Radial gas velocity in the fiducial model with disk buildup as a function of radial distance and time. Blue indicates that the velocity vector is directed toward the central star and red away from it.

vapor is carried outward with the gas flow (see Fig. 4), leading to all CO ice coming from freeze-out. Due to the outward flow of CO vapor, the higher condensation rate is not compensated by evaporation, whose rate is also higher for smaller grains (see Eq. (4)). The higher density of CO ice in the model with buildup ultimately leads to larger grain sizes after 0.5 Myr of evolution (right panel of Fig. 3).

The mass budget analysis shown in Fig. 5 confirms that the difference between the two models revealed by Fig. 2 is primarily associated with enhanced CO freeze-out shortly after the disk reaches its maximum mass. At $t = 0.1$ Myr, the total mass of CO ice is 14 Earth masses higher in the model with disk buildup, and this difference gradually drops to 2 Earth masses at 3 Myr. It is worth noting that the first CO ice is formed just before the disk reaches its maximum mass in this model. Thus, the CO ice component does not yet have a chance to significantly evolve by radial drift. The situation is different for the water ice, the evolution of which starts earlier because of the inside-out buildup pattern. Over 100 Earth masses of water ice are already lost from the disk during the buildup phase. The total mass of water ice becomes practically equal in the two models after the first quarter million years of evolution because the surplus water ice present in the model without disk buildup is lost due to faster

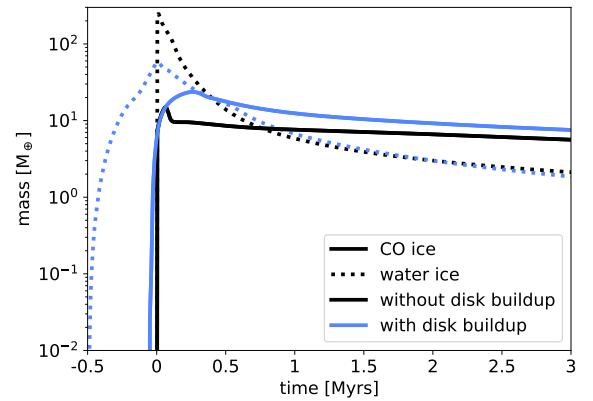


Fig. 5. Time evolution of the total mass of CO ice and water ice (as indicated by the different line styles) in the models with and without disk buildup (indicated with blue and black lines, respectively) for the fiducial set of models.

radial drift caused by faster grain growth. However, the effect of enhanced CO freeze-out on the smaller dust grain sizes caused by the depletion of water ice in the outer disk at the epoch of initial CO ice condensation propagates until the end of the simulation. This occurs because the outer part of the disk, to which the CO ice is confined, is driven not only by the radial drift, but also by the viscous spreading of the disk. As shown in Fig. 4, during all of the evolution, the CO snow line is located outside of the critical radius, so the gas and CO vapor are flowing outward, enhancing the cold-finger effect. This slows down the loss of CO ice compared to the water ice and allows the initial difference to propagate until the end of our model. Our results demonstrate that the CO/H₂O ratio in solids depends on the final disk structure and on the evolutionary path by which the disk formed.

3.2. Lower dust diffusivity and planetesimal formation

As mentioned in the previous subsection, in the fiducial set of models, no planetesimals are formed. This is consistent with the findings of DD18 that show that planetesimal formation is possible if the dust diffusivity is reduced relative to that of the gas. This corresponds to a situation in which the disk midplane,

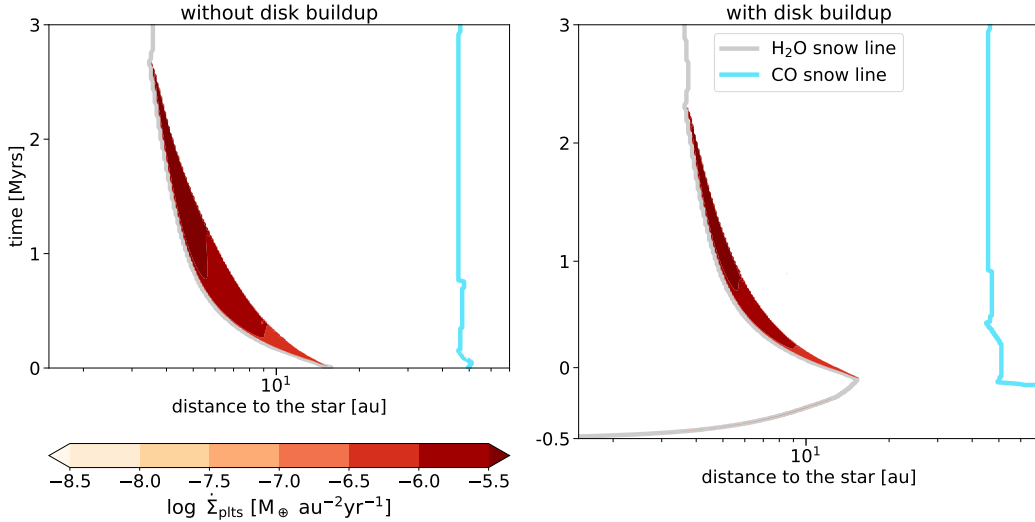


Fig. 6. Planetesimal formation rate as a function of time and space in the models with lower dust diffusivity. The left panel corresponds to the model without disk buildup and the right panel to the model with disk buildup.

where the dust is concentrated, is less turbulent than the disk as a whole. It is a typical assumption made in models dealing with planetesimal formation (see, e.g., [Carrera et al. 2017](#); [Ercolano et al. 2017](#)). To test how the planetesimal formation changes the CO ice enhancement, we performed models with reduced dust diffusivity prescribed as $\alpha_{\text{dust}} = 10^{-5}$, corresponding to the model highlighted in DD18.

Figure 6 shows the planetesimal formation rate in the models without and with disk buildup included. As in DD18, planetesimal formation is only possible outside of the water snow line. The dust-to-gas ratio does not become high enough at the CO snow line to reach the planetesimal formation threshold, which we set to unity. In the model starting with a fully fledged disk, the midplane dust-to-gas ratio reaches 0.9 after 60 000 years of evolution and stays at this level for about 50 000 years, after which it drops and stabilizes at around 0.05. This could grant some planetesimal formation if we used more favorable criteria, i.e., a lower midplane dust-to-gas ratio threshold. For example, [Gole et al. \(2020\)](#) suggested the threshold midplane dust-to-gas ratio of 0.5 based on a set of hydrodynamic models with external turbulence included, and [Carrera et al. \(2025\)](#) suggested the threshold value may be as low as 0.3 if a feedback between dust coagulation and streaming instability is taken into account. In any case, planetesimal formation at the CO snow line would operate only for a limited time and only in the model without disk buildup taken into account. In the model with the dust buildup taken into account, the midplane dust-to-gas ratio reaches its maximum value of 0.25 at around 0.25 Myr after the disk reached its maximum mass. The difference is caused by the dust evolution during the buildup stage, when the water-ice-dominated dust present in the disk before the CO ice could condense had already grown and drifted inward. In addition, planetesimal formation at the water snow line is already active at the buildup stage in this model, binding some pebbles and reducing the amount of dust available overall. A similar conclusion was reached by [Charnoz et al. \(2019\)](#), who presented an analogous model including disk buildup and a dead zone, and did not observe planetesimal formation at the CO snow line.

Figure 7 shows the mass budget of CO ice, water ice, and planetesimals in the model assuming the lower dust diffusivity. The evolution of CO ice is similar to the fiducial model

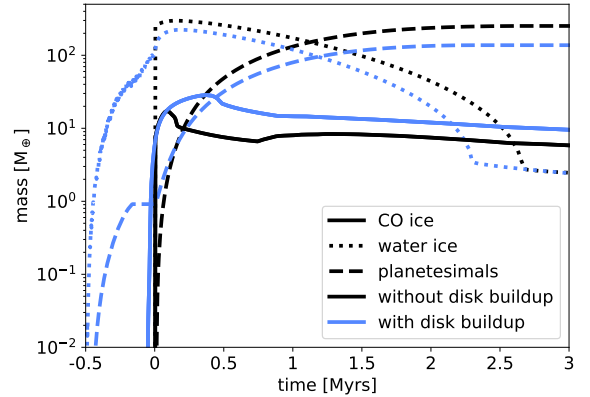


Fig. 7. Time evolution of the total mass of CO ice, water ice, and planetesimals (as indicated by the different line styles) in the models with and without disk buildup (indicated with blue and black lines, respectively) for the set of models with lower dust diffusivity.

(see Fig. 5) as the CO ice is not bound in planetesimals. The evolution of water ice is quite different; in the model with disk buildup about 1 Earth mass of planetesimals already forms along the water snow line during the buildup stage. As in the fiducial model, there is less water ice at the time the model without buildup is initialized, but this time the difference propagates for over 2 Myr. This occurs because the water ice is not only lost to radial drift, but also used for planetesimal formation. However, we limit the planetesimal formation rate such that only part of the available pebbles in the region that fulfill the planetesimal formation criteria are changed into planetesimals. Ultimately, there are about 100 Earth masses more planetesimals formed in the model without disk buildup, and the difference in the water ice budget is erased after planetesimal formation stops at about 2.5 Myr of evolution.

Figure 8 shows that the effect of the CO ice-dominated outer disk is even stronger for the models with low dust diffusivity compared to the fiducial set. Values for CO/H₂O ratios of several hundred, which match the values observed in C/2016 R2, are obtained beyond the CO snow line, both in the model without and with disk buildup. The difference between the models

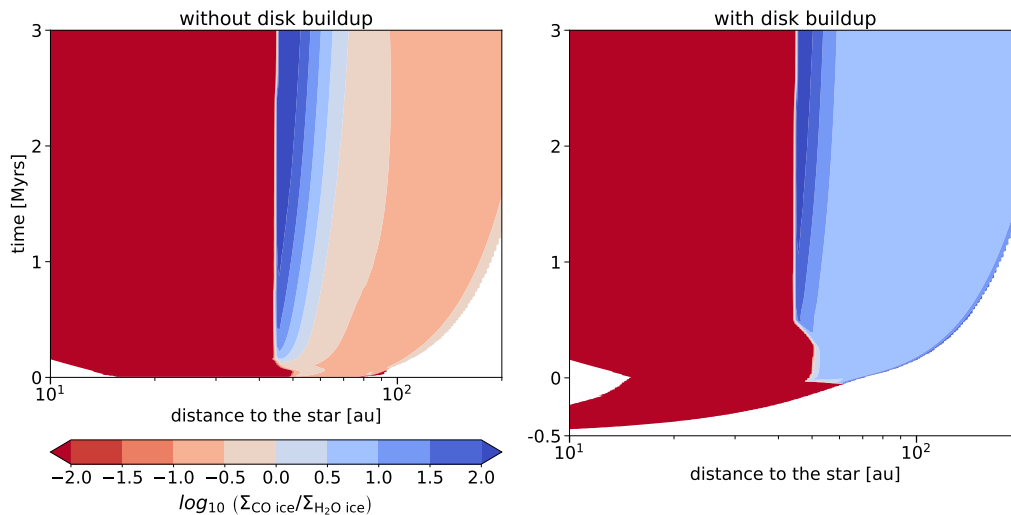


Fig. 8. Evolution of the CO to H₂O ice ratio as a function of time and space in the models with lower dust diffusivity. The left panel corresponds to the model without disk buildup and the right panel to the model with disk buildup.

with and without buildup is more pronounced than in the fiducial set as now both the CO ice augmentation and the water ice depletion play a role. In the model with disk buildup, the region outside of the CO snow line has a CO/H₂O ratio of 5, while in the model without disk buildup the CO/H₂O ratio drops to the fiducial value of 0.28 in the outer disk. However, as discussed above, no CO-rich planetesimals are formed in our models.

4. Discussion

4.1. Limitations of the model

The results presented above are obtained using a one-dimensional model of protoplanetary disk evolution, which necessarily involves a number of simplifying assumptions. While this approach cannot capture non-axisymmetric structures, it allows us to isolate the fundamental effects of disk buildup and dust evolution on water and CO ice abundances.

It should be noted, however, that the buildup model adopted here is rather simplistic. We assume that the initial molecular cloud is spherically symmetric, has a constant density, and rotates as a solid body. Furthermore, we assume that the angular momentum is conserved during the infall. The current observations and models of star-forming environments paint a more complex picture, with filamentary structures leading to heterogeneous accretion on disks (Kuffmeier et al. 2017; Lee et al. 2021; Pineda et al. 2023; Bhandare et al. 2024). It is not excluded that the infall itself leads to producing a disk with substructure able to impact the dust evolution and planetesimal formation (Kuznetsova et al. 2022; Hühn et al. 2025; Zhao et al. 2025).

In the model we keep the luminosity of the central star constant. The evolution of the stellar luminosity would not have much impact on the location of the water snow line, which is located in the region dominated by viscous heating, but would have an effect on the location of the CO line, which is in the outer disk where the temperature is set by stellar irradiation (Miley et al. 2021). In the models presented by Price et al. (2021) that included the stellar luminosity evolution, the CO snow line moves inward with time. The inward movement of the CO line could lead to a lower efficiency of the cold-finger process with time, but should not significantly impact the results presented here.

Our model neglects the trapping of CO ice in amorphous water ice or clathrates found in laboratory experiments (Bar-Nun et al. 1985; Zhou et al. 2024; Ligterink et al. 2024; Pesciotta et al. 2024). This effect can increase the effective binding energy of CO and partially couple its evolution to that of water (Williams et al. 2025). Including this process would likely reduce the degree of CO to water fractionation by allowing a fraction of CO to be removed together with drifting water-rich pebbles. However, because CO trapping requires the presence of water ice, its efficiency is expected to decrease in the models including infall, as early dust growth and drift progressively deplete the disk of water ice. Therefore, one can expect the qualitative trend of enhanced CO/H₂O ratios produced during disk buildup to be robust, although the absolute enrichment may be reduced.

We neglected chemical conversion of CO, which may be efficient in warm UV-irradiated surface layers of the protoplanetary disk. However, chemical models show that CO conversion is expected to proceed slowly in the cold midplane regions considered here (Eistrup et al. 2018; Bosman et al. 2018; Van Clepper et al. 2022).

4.2. Planetesimal formation beyond the CO snow line

CO-rich pebbles are formed at the CO snow line in the models, both with and without disk buildup. However, these pebbles do not participate in planetesimal formation, which only happens at the water snow line in the models assuming low dust diffusivity. Consequently, our model does not produce planetesimals with a high CO/H₂O ratio that could be precursors of CO-rich comets such as C/2016 R2. Such bodies could potentially be produced if the infall was not homogeneous and triggered pressure traps in the disk (Kuznetsova et al. 2022; Hühn et al. 2025; Zhao et al. 2025).

CO-rich bodies could also form as second-generation planetesimals. Our current model does not include the possibility of planetesimals growing into planets. If the planetesimals that formed at the water snow line can form a massive planetary core that starts gas accretion and opens a gap in the disk, the outer edge of the planetary gap would act as a pressure bump that stops the pebble drift and induces planetesimal formation in the outer disk (Eriksson et al. 2020; Shibaïke & Alibert 2020; Lau et al. 2024). Recently, Lau et al. (2025) showed that the

combination of giant planet formation in the outer disk and disk dispersal by photoevaporation can lead to a late burst of planetesimal formation in the outer disk that will bind the leftover pebbles in planetesimals. In addition, photoevaporation alone, even in the absence of a planet-induced gap, may create pressure gradients capable of concentrating solids and promoting planetesimal formation (Carrera et al. 2017; Ercolano et al. 2017; Ying et al. 2026). These late-formed planetesimals would be spared the internal heating and processing by the short-lived radioactive isotopes, consistent with the properties of comets (Priyalnik et al. 1987). Thus, the CO-rich pebbles could turn into planetesimals if the full picture of planet formation and disk dispersal is taken into account, which is a motivation for future work on connecting disk evolution, planet formation, and chemistry.

5. Conclusions

In this work we analyzed the prospect of forming planetesimals enriched in CO ice that could be the parent bodies of comets, such as the comet C/2016 R2 (PanSTARRS). We found that pebbles with a very high CO/H₂O, matching the value of 300 observed in C/2016 R2, can form due to the cold-finger effect outside of the CO snow line if the dust diffusivity is low. In the models including disk buildup, the whole region outside of the CO snow line becomes dominated by CO ice with CO/H₂O ratios ranging from 3 to 5, depending on dust diffusivity. However, these CO-rich pebbles do not become planetesimals in our models. Planetesimals only form along the water snow line, as the dust-to-gas ratio is never high enough for planetesimal formation at the CO snow line. This suggests that CO-rich planetesimals may form preferentially as second-generation bodies, after CO enrichment has occurred and if solid concentrations are locally enhanced. Such enhancement could occur in pressure bumps, planet-induced gaps, or regions affected by photoevaporative gas removal, but these mechanisms were not modeled here.

Comparing the standard model starting with a fully fledged protoplanetary disk and initialized with a constant dust-to-gas ratio to models including disk buildup, we found significant differences regarding the CO/H₂O ratio of pebbles in the outer disk. Dust evolution during the earliest stages of disk buildup leads to a lower water ice abundance, smaller grain size, and augmented CO condensation compared to the prediction of a model not including disk buildup. Similar behavior should be expected for other volatiles. Thus, models dealing with the chemical evolution of the disk should consider the buildup stage in the efforts of constraining planetary formation from the observed atmospheric molecular ratios such as C/O (see, e.g., Öberg et al. 2011; Booth et al. 2017; Krijt et al. 2020; Schneider & Bitsch 2021; Houge et al. 2025; Guzmán Franco et al. 2026).

Acknowledgements. J.D. thanks the anonymous referee for constructive comments that helped to improve this paper. J.D. was funded by the European Union under the European Union's Horizon Europe Research & Innovation Programme 101040037 (PLANETOIDS). Views and opinions expressed are however those of the author only and do not necessarily reflect those of the European Union or the European Research Council. Neither the European Union nor the granting authority can be held responsible for them.

References

Bar-Nun, A., Herman, G., Laufer, D., & Rappaport, M. L. 1985, *Icarus*, **63**, 317
Bhandare, A., Commerçon, B., Laibe, G., et al. 2024, *A&A*, **687**, A158

- Birnstiel, T., Dullemond, C. P., & Brauer, F. 2010, *A&A*, **513**, A79
Birnstiel, T., Klahr, H., & Ercolano, B. 2012, *A&A*, **539**, A148
Biver, N., Bockelée-Morvan, D., Paubert, G., et al. 2018, *A&A*, **619**, A127
Bodewits, D., Noonan, J. W., Feldman, P. D., et al. 2020, *Nat. Astron.*, **4**, 867
Boney, B. P., Villanueva, G. L., DiSanti, M. A., et al. 2017, *AJ*, **153**, 241
Booth, R. A., Clarke, C. J., Madhusudhan, N., & Ilee, J. D. 2017, *MNRAS*, **469**, 3994
Bosman, A. D., Walsh, C., & van Dishoeck, E. F. 2018, *A&A*, **618**, A182
Brearley, A. J. 2006, in *Meteorites and the Early Solar System II*, eds. D. S. Lauretta, & H. Y. McSween (Tucson: University of Arizona Press), 584
Carrera, D., Gorti, U., Johansen, A., & Davies, M. B. 2017, *ApJ*, **839**, 16
Carrera, D., Lim, J., Eriksson, L. E. J., Lyra, W., & Simon, J. B. 2025, *A&A*, **696**, L23
Charnoz, S., Pignatale, F. C., Hyodo, R., et al. 2019, *A&A*, **627**, A50
Cleeves, L. I., Bergin, E. A., Alexander, C. M. O. D., et al. 2014, *Science*, **345**, 1590
Cordiner, M. A., Milam, S. N., Biver, N., et al. 2020, *Nat. Astron.*, **4**, 861
De Prá, M. N., Hénault, E., Pinilla-Alonso, N., et al. 2025, *Nat. Astron.*, **9**, 252
Drażkowska, J., & Alibert, Y. 2017, *A&A*, **608**, A92
Drażkowska, J., & Dullemond, C. P. 2018, *A&A*, **614**, A62
Eistrup, C., Walsh, C., & van Dishoeck, E. F. 2018, *A&A*, **613**, A14
Ercolano, B., Jennings, J., Rosotti, G., & Birnstiel, T. 2017, *MNRAS*, **472**, 4117
Eriksson, L. E. J., Johansen, A., & Liu, B. 2020, *A&A*, **635**, A110
Feaga, L. M., A'Hearn, M. F., Farnham, T. L., et al. 2014, *AJ*, **147**, 24
Gole, D. A., Simon, J. B., Li, R., Youdin, A. N., & Armitage, P. J. 2020, *ApJ*, **904**, 132
Guzmán Franco, A. D., Savvidou, S., & Bitsch, B. 2026, *A&A*, **707**, A276
Harrington Pinto, O., Womack, M., Fernandez, Y., & Bauer, J. 2022, *Planet. Sci. J.*, **3**, 247
Houge, A., Johansen, A., Bergin, E., et al. 2025, *A&A*, **699**, A227
Hueso, R., & Guillot, T. 2005, *A&A*, **442**, 703
Hühn, L.-A., Dullemond, C. P., Lebreuilly, U., et al. 2025, *A&A*, **696**, A162
Krijt, S., Bosman, A. D., Zhang, K., et al. 2020, *ApJ*, **899**, 134
Kuffmeier, M., Haugbølle, T., & Nordlund, Å. 2017, *ApJ*, **846**, 7
Kuznetsova, A., Bae, J., Hartmann, L., & Mac Low, M.-M. 2022, *ApJ*, **928**, 92
Lau, T. C. H., Birnstiel, T., Drażkowska, J., & Stammer, S. M. 2024, *A&A*, **688**, A22
Lau, T. C. H., Birnstiel, T., Stammer, S. M., & Drażkowska, J. 2025, *ApJ*, **994**, 74
Lee, Y.-N., Charnoz, S., & Hennebelle, P. 2021, *A&A*, **648**, A101
Leger, A., Jura, M., & Omont, A. 1985, *A&A*, **144**, 147
Ligterink, N. F. W., Kipfer, K. A., & Gavino, S. 2024, *A&A*, **687**, A224
Lodders, K. 2003, *ApJ*, **591**, 1220
Marrocchi, Y., Bekaert, D. V., & Piani, L. 2018, *Earth Planet. Sci. Lett.*, **482**, 23
McKay, A. J., DiSanti, M. A., Kelley, M. S. P., et al. 2019, *AJ*, **158**, 128
Miley, J. M., Panić, O., Booth, R. A., et al. 2021, *MNRAS*, **500**, 4658
Mousis, O., Lunine, J. I., Picaud, S., & Cordier, D. 2010, *Faraday Discuss.*, **147**, 509
Mousis, O., Aguichine, A., Bouquet, A., et al. 2021, *Planet. Sci. J.*, **2**, 72
Öberg, K. I., Murray-Clay, R., & Bergin, E. A. 2011, *ApJ*, **743**, L16
Pesciotta, C., Simon, A., Rajappan, M., & Öberg, K. I. 2024, *ApJ*, **973**, 166
Pineda, J. E., Arzoumanian, D., Andre, P., et al. 2023, *ASP Conf. Ser.*, **534**, 233
Pinilla-Alonso, N., Brunetto, R., De Prá, M. N., et al. 2025, *Nat. Astron.*, **9**, 230
Priyalnik, D., Bar-Nun, A., & Podolak, M. 1987, *ApJ*, **319**, 993
Price, E. M., Cleeves, L. I., Bodewits, D., & Öberg, K. I. 2021, *ApJ*, **913**, 9
Schneider, A. D., & Bitsch, B. 2021, *A&A*, **654**, A71
Schoonenberg, D., & Ormel, C. W. 2017, *A&A*, **602**, A21
Shibaike, Y., & Alibert, Y. 2020, *A&A*, **644**, A81
Shu, F. H. 1977, *ApJ*, **214**, 488
Sridhar, S., Bryson, J. F. J., King, A. J., & Harrison, R. J. 2021, *Earth Planet. Sci. Lett.*, **576**, 117243
Stammer, S. M., Birnstiel, T., Panić, O., Dullemond, C. P., & Dominik, C. 2017, *A&A*, **600**, A140
Ulrich, R. K. 1976, *ApJ*, **210**, 377
Van Clepper, E., Bergner, J. B., Bosman, A. D., Bergin, E., & Ciesla, F. J. 2022, *ApJ*, **927**, 206
Visser, R., van Dishoeck, E. F., Doty, S. D., & Dullemond, C. P. 2009, *A&A*, **495**, 881
Williams, J., Krijt, S., Bitsch, B., Houge, A., & Bergner, J. 2025, *MNRAS*, **544**, 3562
Ying, X., Liu, B., Yang, H., et al. 2026, *A&A*, **707**, A223
Zhao, H., Lau, T. C. H., Birnstiel, T., Stammer, S. M., & Drażkowska, J. 2025, *A&A*, **694**, A205
Zhou, Q., Simon, A., Öberg, K. I., & Rajappan, M. 2024, *ApJ*, **972**, 189